

BOOSTING MR IMAGE IMPULSE NOISE REMOVAL WITH OVERLAPPING GROUP SPARSE FRACTIONAL-ORDER TOTAL VARIATION AND MINIMAX CONCAVE PENALTY

WEI XUE¹, YUMENG GE¹, XIAOLEI GU², XUAN QI² AND TAO TAO^{✉,1}

¹School of Computer Science and Technology, Anhui University of Technology, Maanshan 243032, China,

²Department of Radiology, Maanshan People's Hospital, Maanshan 243099, China

e-mail: xuewei@ahut.edu.cn; geyumeng2@foxmail.com; guxiaolei88@sina.com; drqi50731@163.com; taotao@ahut.edu.cn

(Received January 19, 2024; revised March 1, 2024; accepted March 1, 2024)

ABSTRACT

The acquisition and transmission of magnetic resonance images are susceptible to noise, particularly impulse noise. Although the method based on the ℓ_0 -norm and overlapping group sparse total variation (ℓ_0 -OGSTV) is effective for impulse noise image restoration, it can only mitigate the staircase artifacts to a certain extent. To boost the impulse noise removal performance of ℓ_0 -OGSTV, we propose a new restoration model that consists of two terms. Specifically, in the first term, we keep using the ℓ_0 -norm as the data fidelity term to eliminate impulse noise. In the second term, we first introduce an overlapping group sparsity fractional-order total variation regularizer to eliminate staircase artifacts while preserving structural information. Then, we adopt the minimax-concave penalty to further accurately estimate the image edges. Finally, we employ an alternate direction method of multipliers to solve the proposed optimization model. Clinical experiments demonstrate its effectiveness in denoising medical images.

Keywords: fractional-order total variation, image denoising, ℓ_0 -norm, minimax-concave penalty, overlapping group sparsity.

INTRODUCTION

Due to the reasons of acquisition technology and system, noise and artifacts are introduced in magnetic resonance (MR) images, and impulse noise is one of the main noises. The impulse noise may be misunderstood as an anomaly of the human health system, and denoising can enrich the visual quality of images. Denoising plays a crucial role in medical imaging and scanning, where even a small amount of noise can be misinterpreted as an anomaly in the human health system. However, removing noise is a complex process because it can sometimes compromise the visual effect and details of the image. Therefore, the restoration of MR images destroyed by impulse noise has become a prominent area of research in the field of image processing.

Many methods have been proposed for medical image denoising, one of the most popular image restoration methods is total variation (TV) model

(Rudin *et al.*, 1992), which could preserve edges and remove image noise in homogeneous regions. However, it tended to produce staircase artifacts in smooth regions. To solve this problem, various solutions have been proposed. For example, high-order TV methods (Adam *et al.*, 2021; Ge *et al.*, 2023), the overlapping group sparsity total variation (OGSTV) methods (Liu *et al.*, 2014; Shi *et al.*, 2016), fractional TV methods (Lian and Liu, 2023; Rahman Chowdhury *et al.*, 2020; Zhu *et al.*, 2022) and the minimax-concave (MC) penalty methods (Du and Liu, 2018; Chen and Zhao, 2023).

Among these methods, the OGSTV method excels in image restoration due to its structural sparsity. In (Ge *et al.*, 2023), a method that combined the hyper-Laplacian prior regularization with OGSTV and non-convex second-order TV, performed well in removing noise from MR images. Ji and Zhao (2023) proposed a novel model with a non-convex penalty that combined

the OGS regularizer and the MC penalty (OGS-MCTV). The non-convex MC penalty could preserve edges. Therefore, this method demonstrated a superior image denoising effect compared to other models. Bhutto *et al.* (2023) proposed an image denoising algorithm that cleverly integrated the advantages of the fractional-order variation domain with an OGS measure, which acted as its regularization component. The fidelity term of these models used the ℓ_2 -norm, which is commonly used to restore images degraded by additive Gaussian noise. In addition, the ℓ_2 -norm is sensitive to outliers and can easily result in unsatisfactory image restoration.

To effectively remove impulse noise, as described in (Gao *et al.*, 2018), Bayesian statistical rules suggested that the ℓ_1 -norm fidelity was more suitable for restoring images corrupted by impulse noise than the ℓ_2 -norm. In (Yang *et al.*, 2009), the fidelity term of the ℓ_1 -norm was utilized to restore the fuzzy multi-channel image damaged by impulse noise. Chan *et al.* (2010) proposed a two-phase image restoration method based on TV regularization combined with the ℓ_1 -norm data fidelity term for impulse noise removal. Numerical results proved that the proposed method makes good progress in restoration capability. Although the ℓ_1 -norm has demonstrated significant advantages in sparse signal processing and image restoration, it may overly penalize the obtained solution in impulse noise removal (Kuang *et al.*, 2018).

To address the aforementioned issues, a method for removing impulse noise using ℓ_0 total variation (ℓ_0 -TV) was proposed in (Yuan and Ghanem, 2017). It can be depicted as

$$\min_u \|o \odot (Ku - f)\|_0 + \lambda \phi_{TV}(u) \quad (1)$$

where $u \in \mathbb{R}^{n \times m}$ is the desired original clean image, $f \in \mathbb{R}^{n \times m}$ is the degraded image, $\lambda > 0$ is the regularization parameter, $o \in \{0, 1\}^n$ is specified by the user, \odot denotes an elementwise product, $K \in \mathbb{R}^{n \times n}$ is a linear operator. In this paper, we are concerned with $K = I$, the identity operator, which constitutes a denoising problem.

Recently, the ℓ_0 -norm data fidelity term has been used to remove impulse noise in (Yin *et al.*, 2022). The

OGSTV serves as a regularizer to effectively eliminate staircase artifacts, making this model highly proficient in image restoration tasks even under high impulse noise levels. Sun and Liu (2023) integrated both the ℓ_0 -norm data fidelity term and the nonconvex generalized regularizer, demonstrating not its remarkable ability to suppress impulse noise and its superior capability in preserving sharp contours while reducing staircase artifacts. These models collectively demonstrate the suitability of ℓ_0 -norm for restoring images corrupted by impulse noise.

According to the literature survey above, the existing methods primarily focus on restoring natural images. However, when it comes to medical image restoration, more emphasis is placed on preserving intricate textures to ensure clinical diagnostic value. Therefore, this paper primarily investigates boosting MR image impulse noise removal. The model comprises an ℓ_0 -norm data fidelity term, a regularizer of overlapping group sparse fractional-order total variation (OGS-FOTV) and the MC penalty. Our proposed method combines the advantages of the fractional-order variation domain with the OGS measure, which can effectively measure complex texture details and reduce staircase artifacts. Additionally, the MC penalty can improve the sparsity of images in the gradient domain and improve the estimation of high-frequency components, that is, preserve edges. To address the computational challenges stemming from the model's complexity, we employ the alternate direction multiplier algorithm to solve the subproblems. Finally, we conduct numerical experiments to analyze the effectiveness of our proposed model.

The rest of this article is organized as follows. Section 2 presents some elementary concepts and preliminaries related to the proposed algorithm. In Section 3, we propose a new model for impulse noise removal and derive an efficient algorithm to solve the corresponding minimization problem. In Section 4, the superiority of the proposed method is proved by numerical experiments. Finally, a conclusion is made in Section 5.

PRELIMINARIES

In order to better describe the model, in this section, we introduce the definition of the ℓ_0 fidelity term, the Moreau envelope, the MC penalty, overlapping group sparsity, discrete fractional-order difference and the ADMM framework.

THE ℓ_0 FIDELITY TERM

First, we give some basic definitions and properties related to the ℓ_0 -norm fidelity term. The $o \in \{0, 1\}^n$ is specified by the user. More specifically, when $o_i = 0$, the pixel at position i is an outlier, and when $o_i = 1$, the pixel at position i is a potential outlier. For this paper, we set $o_i = \begin{cases} 0, & f_i = u_{min} \text{ or } u_{max} \\ 1, & \text{otherwise} \end{cases}$ for the salt-and-pepper impulse noise.

The following lemma, as delineated in (Yuan and Ghanem, 2017), presents the variational characterization of the ℓ_0 -norm.

Lemma 1 For any given $w \in \mathbb{R}^n$, it holds that

$$\|w\|_0 = \min_{0 \leq z \leq 1} \langle 1, 1 - z \rangle, \quad s.t. \quad z \odot |w| = 0, \quad (2)$$

and $z^* = 1 - \text{sign}(|w|)$ is the unique optimal solution to problem (2). Here, the standard signum function sign is employed in component form, and $\text{sign}(0) = 0$.

THE MINIMAX-CONCAVE PENALTY

Definition 1 Let $b \geq 0$, we define $\varphi_b(x) : \mathbb{R}^N \rightarrow \mathbb{R}$ as the Moreau envelope of function f (Selesnick, 2017)

$$\varphi_b(x) = \min_v \left\{ \frac{b}{2} \|x - v\|_2^2 + f(v) \right\} \quad (3)$$

The Moreau envelope is convex, continuous, differentiable and real valued (Zhou and Zhao, 2021).

Definition 2 Let $b \geq 0$, the minimax-concave penalty of $\|x\|_2$ with parameter b is the function $\hat{\varphi}_b(x) : \mathbb{R}^N \rightarrow \mathbb{R}$ which is given by (Du and Liu, 2018)

$$\hat{\varphi}_b(x) = \|x\|_2 - \min_v \left\{ \frac{b}{2} \|x - v\|_2^2 + \|v\|_2 \right\} \quad (4)$$

where the function $\hat{\varphi}_b(x)$ is non-convex (Ji and Zhao, 2023; Shen et al., 2021).

OVERLAPPING GROUP SPARSITY

Liu et al. (2015; 2014) expanded the OGSTV function as a new regularizer from the one-dimensional signal denoising problem (Selesnick and Chen, 2013) to the general two-dimensional case. This approach effectively reduces staircase artifacts. They also defined a $K \times K$ point group of the image $g \in \mathbb{R}^{n^2}$.

$$\tilde{g}_{i,j,K} = \begin{bmatrix} g_{i-m_l, j-m_l} & g_{i-m_l, j-m_l+1} & \cdots & g_{i-m_l, j+m_r} \\ g_{i-m_l+1, j-m_l} & g_{i-m_l+1, j-m_l+1} & \cdots & g_{i-m_l+1, j+m_r} \\ \vdots & \vdots & \ddots & \vdots \\ g_{i+m_r, j-m_l} & g_{i+m_r, j-m_l+1} & \cdots & g_{i+m_r, j+m_r} \end{bmatrix} \in \mathbb{R}^{K \times K}, \quad (5)$$

where $m_l = \lfloor \frac{K-1}{2} \rfloor, m_r = \lfloor \frac{K}{2} \rfloor$ and $\lfloor x \rfloor$ denotes the largest integer less than or equal to x . The center of $\tilde{g}_{i,j,K}$ is (i, j) . Let $g_{i,j,K}$ be a vector which is obtained by stacking the K columns of the matrix $\tilde{g}_{i,j,K}$, i.e., $g_{i,j,K} = \tilde{g}_{i,j,K}(\cdot)$. Then the OGS regularizer can be defined by

$$\phi_{OT}(g) = \sum_{i,j=1}^K \|g(i, j)_K\|_2 \quad (6)$$

DEFINITION OF DISCRETE FRACTIONAL-ORDER DIFFERENCE

There exist multiple interpretations of fractional differences, and the Grünwald-Letnikov (G-L) fractional-order derivative (Zhang et al., 2012) is among the prevalent methods. Defined by G-L, let the size of an image u be $N \times M$. Thus, the discrete form of the fractional-order gradient $\nabla^\alpha u$ can be evaluated by

$$\nabla^\alpha u = [D_x^\alpha u, D_y^\alpha u], \quad (7)$$

where α is the fractional order and we set $1 \leq \alpha < 2$ in this paper. The discrete gradients $D_x^\alpha u, D_y^\alpha u \in \mathbb{R}^{N \times M}$ along the x -axis and the y -axis are given by

$$\begin{cases} (D_x^\alpha u)_{i,j} = \sum_{k=0}^{K-1} (-1)^k C_k^\alpha u_{i-k,j} \\ (D_y^\alpha u)_{i,j} = \sum_{k=0}^{K-1} (-1)^k C_k^\alpha u_{i,j-k} \end{cases} \quad (8)$$

with $1 \leq i \leq N, 1 \leq j \leq M$. Here K is the number of adjacent pixels that are used to calculate the fractional-order derivative at each pixel. The coefficients $\{C_k^\alpha\}_{k=0}^{K-1}$ are given by $C_k^\alpha = \frac{\Gamma(\alpha+1)}{\Gamma(k+1)\Gamma(\alpha+1-k)}$ with the Gamma function $\Gamma(x)$. Furthermore, the conjugate operator of the fractional-order gradient operator is $(\nabla^\alpha)^* = \overline{(-1)^\alpha} \text{div}^\alpha$. In the discrete case, the vector $p = (p^{(1)}, p^{(2)}) \in \mathbb{R}^{N \times M} \times \mathbb{R}^{N \times M}$ discrete fractional-order divergence is defined as (Rahman Chowdhury *et al.*, 2020; Bhutto *et al.*, 2023)

$$(\text{div}^\alpha p)_{i,j} = (-1)^\alpha \sum_{k=0}^{K-1} (-1)^k C_k^\alpha (p_{i+k,j}^{(1)} + p_{i,j+k}^{(2)}). \quad (9)$$

THE ALTERNATING DIRECTION METHOD OF MULTIPLIERS

The alternating direction method of multipliers (ADMM) is to solve the following constrained separable optimization problems:

$$\min_{x,y} \xi_1(x) + \xi_2(y) \quad \text{s.t. } Ax + By = d, \quad x, y \in \mathcal{X}_i \quad (10)$$

where $\xi_i(\cdot) : \mathcal{X}_i \rightarrow \mathbb{R}$ are closed convex functions, $A, B \in \mathbb{R}^{l \times n}$ and $d \in \mathbb{R}^l$ is a given vector. The augmented Lagrangian function (Hestenes, 1969) for the problem (10) is

$$\begin{aligned} \mathcal{L}_{\mathcal{A}}(x, y; \mu) &= \xi_1(x) + \xi_2(y) + \mu^T (Ax + By - d) \\ &\quad + \frac{\delta}{2} \|Ax + By - d\|_2^2, \end{aligned} \quad (11)$$

where $\mu \in \mathbb{R}^l$ is the Lagrange multiplier and $\delta > 0$ is a penalty parameter. The objective is to find the saddle point of $\mathcal{L}_{\mathcal{A}}$ by alternatively minimizing $\mathcal{L}_{\mathcal{A}}$ with respect to x, y and μ . The ADMM algorithm to solve problem (10) is presented as Algorithm 1.

Algorithm 1 ADMM for minimizing the problem (10).

- 1: initialization x^0, y^0, λ^0 and $\delta > 0$,
 - 2: iteration:
 - $x^{k+1} = \arg \min_x \xi_1(x) + \frac{\delta}{2} \|Ax + By^k - d + \frac{\mu^k}{\delta}\|_2^2$,
 - $y^{k+1} = \arg \min_y \xi_2(y) + \frac{\delta}{2} \|Ax^{k+1} + By - d + \frac{\mu^k}{\delta}\|_2^2$,
 - $\mu^{k+1} = \mu^k + \delta(Ax^{k+1} + By^{k+1} - d)$,
 - $k = k + 1$
 - 3: until a stopping criterion is satisfied.
-

THE PROPOSED ALGORITHM

In this section, we first introduce the proposed MR Image denoising model, and then solve it in the ADMM framework.

MODEL

The proposed MR Image denoising model is as follows

$$\min_u \|o \odot (u - f)\|_0 + \Phi_b^K(u), \quad (12)$$

where $\Phi_b^K(u)$ is a new non-convex penalty based on the MC penalty (Ji and Zhao, 2023) and the overlapping group sparse fractional-order total variation (OGS-FOTV) (Bhutto *et al.*, 2023), which is defined as follows

Definition 3 Let $\lambda_1, \lambda_2 \geq 0, 1 \leq \alpha < 2$, we define $\Phi_b^K(u) : \mathbb{R}^{N \times N} \rightarrow \mathbb{R}$ with parameter λ_1, λ_2 as follows

$$\begin{aligned} \Phi_b^K(u) &= \lambda_1 \sum_{i,j=1}^N \|[\nabla^\alpha u]_{i,j,K}\|_2 - \\ &\quad \lambda_2 \sum_{i,j=1}^N \min_{v_{i,j,K}} \left\{ \frac{b}{2} \|[\nabla^\alpha u]_{i,j,K} - v_{i,j,K}\|_2^2 + \|v_{i,j,K}\|_2 \right\} \\ &= \lambda_1 \phi(\nabla^\alpha u) - \lambda_2 \min_v \left\{ \frac{b}{2} \|\nabla^\alpha u - v\|_2^2 + \phi(v) \right\} \end{aligned} \quad (13)$$

where $\phi(\cdot)$ is the OGS regularizer as defined by Eq. (6). And $\phi(\nabla^\alpha u)$ represents the OGS-FOTV regularizer, $\nabla^\alpha u$ is the fractional-order gradient as defined by Eq. (7).

Next, according to Eq. (13), we proposed model (12) can be reformulated as

$$\begin{aligned} \min_u \left\{ \|o \odot (u - f)\|_0 + \left[\lambda_1 \phi(\nabla^\alpha u) \right. \right. \\ \left. \left. - \lambda_2 \min_v \left(\frac{b}{2} \|\nabla^\alpha u - v\|_2^2 + \phi(v) \right) \right] \right\} \end{aligned} \quad (14)$$

OPTIMIZATION

We use the variable splitting method together with Lemma 1 to transform problem (14) into the following

constrained optimization problem

$$\begin{aligned} \min_{u,z,x} \max_v & \langle 1, 1-v \rangle + \lambda_1 \phi(x) - \frac{b\lambda_2}{2} \|x-v\|_2^2 - \lambda_2 \phi(v) \\ \text{s.t. } & x = \nabla^\alpha u, y = u - f, z \odot |o \odot y| = z \odot o \odot |y| = 0. \end{aligned} \quad (15)$$

To solve (15), we adopt ADMM (Boyd *et al.*, 2011; Wang *et al.*, 2019) and transform Eq. (15) into the following augmented Lagrangian function

$$\begin{aligned} \mathcal{L}_{\mathcal{A}}(u, z, x, y; \mu, \delta, \eta) \\ = & \langle 1, 1-v \rangle + \lambda_1 \phi(x) - \frac{b\lambda_2}{2} \|x-v\|_2^2 - \lambda_2 \phi(v) + \\ & \langle \nabla^\alpha u - x, \mu \rangle + \frac{\beta_1}{2} \|\nabla^\alpha u - x\|_2^2 + \langle u - f - y, \delta \rangle + \\ & \frac{\beta_2}{2} \|u - f - y\|_2^2 + \langle z \odot o \odot |y|, \eta \rangle + \frac{\beta_3}{2} \|z \odot o \odot |y|\|_2^2 \end{aligned} \quad (16)$$

where μ, δ, η are Lagrangian multipliers, $\beta_1, \beta_2, \beta_3$ are penalty parameters. To solve Eq. (15), we utilize the ADMM framework and iteratively update each variable by minimizing Eq. (16). This iterative process can be decomposed into several subproblems.

u-subproblem

The u-subproblem

$$\begin{aligned} u^{k+1} &= \arg \min_u \frac{\beta_1}{2} \|\nabla^\alpha u - x^k\|_2^2 + \langle \nabla^\alpha u - x^k, \mu^k \rangle \\ &+ \frac{\beta_2}{2} \|u - f - y^k\|_2^2 + \langle u - f - y^k, \delta^k \rangle \\ &= \arg \min_u \frac{\beta_1}{2} \left\| \nabla^\alpha u - x^k + \frac{\mu^k}{\beta_1} \right\|_2^2 \\ &+ \frac{\beta_2}{2} \left\| u - f - y^k + \frac{\delta^k}{\beta_2} \right\|_2^2 \end{aligned} \quad (17)$$

Subproblem (17) is a least squares problem, we can solve the equivalent normal equation,

$$\begin{aligned} (\beta_1 (\nabla^\alpha)^T (\nabla^\alpha) + \beta_2 I) u = \\ (\nabla^\alpha)^T (\beta_1 x^k - \mu^k) + \beta_2 y^k + \beta_2 f - \delta^k \end{aligned} \quad (18)$$

For the periodic boundary condition of u , $(\nabla^\alpha)^T \nabla^\alpha$ is the block circulant with circulant blocks, which can be diagonalized by 2D discrete Fourier transform (Wu and Tai, 2010). Therefore, through a fast Fourier transform (FFT) operation and a FFT inverse

operation, we can obtain the optimal u as follows

$$u^{k+1} = \mathcal{F}^{-1} \left(\frac{\mathcal{F}[(\nabla^\alpha)^T (\beta_1 x^k - \mu^k) + \beta_2 y^k + \beta_2 f - \delta^k]}{\beta_2 I + \beta_1 \mathcal{F}[(\nabla^\alpha)^T (\nabla^\alpha)]} \right) \quad (19)$$

x-subproblem

The x-subproblem is the overlapping group sparse problem, we have

$$\begin{aligned} x^{k+1} &= \arg \min_x \lambda_1 \phi(x) - \frac{b\lambda_2}{2} \|x - v^k\|_2^2 + \langle \nabla^\alpha u - x^k, \mu^k \rangle \\ &+ \frac{\beta_1}{2} \|\nabla^\alpha u - x^k\|_2^2 \\ &= \arg \min_x \frac{\beta_1 - b\lambda_2}{2} \left\| x - \frac{\beta_1 \nabla^\alpha u - b\lambda_2 v^k + \mu^k}{\beta_1 - b\lambda_2} \right\|_2^2 \\ &+ \lambda_1 \phi(x) \end{aligned} \quad (20)$$

The problem (12) can be solved iteratively by the majorization-minimization (MM) algorithm, and the process of solving the related problem is discussed in detail in (Yin *et al.*, 2022). Here, we express it in lemma 2, as follows

Lemma 2 we consider a minimization problem of the form $\min_v P(v) = \frac{1}{2} \|v - v_0\|_2^2 + \rho \Phi(v)$, where ρ is a positive parameter and the functional $\Phi(v) = \sum_{i,j=1}^n \|g_{(i,j),K}\|_2$. In order to minimize $P(v)$, the MM algorithm is continuously iteratively solved to obtain

$$v^{k+1} = \left(I + \rho \Lambda(v^k)^T \Lambda(v^k) \right)^{-1} v_0 \quad (21)$$

v-subproblem

The v subproblem can be written as

$$\begin{aligned} v^{k+1} &= \arg \max_v \left\{ -\frac{b\lambda_2}{2} \|x^{k+1} - v\|_2^2 - \lambda_2 \phi(v) \right\} \\ &= \arg \min_v \frac{b\lambda_2}{2} \|x^{k+1} - v\|_2^2 + \lambda_2 \phi(v) \end{aligned} \quad (22)$$

The algorithm for v-subproblem is the same as the algorithm for x-subproblem.

z-subproblem

The z-subproblem is of the following form

$$z^{k+1} = \arg \min_z \frac{1}{2} \beta_3 o \odot y^k \odot y^k \odot z^2 + (\eta^k \odot o \odot |y^k| - 1)z \quad (23)$$

The solution z^{k+1} can be computed using projection as:

$$z^{k+1} = \min \left\{ 1, \max \left(-\frac{\eta^k \odot o \odot |y^k| - 1}{\beta_3 o \odot y^k \odot y^k}, 0 \right) \right\} \quad (24)$$

y-subproblem

The y-subproblem can be solved by a soft thresholding with the shrink operator. Besides, this subproblem shares the following form

$$y^{k+1} = \arg \min_y \frac{\beta_2}{2} \left\| y - \left(u^{k+1} - f + \frac{\delta^k}{\beta_2} \right) \right\|_2^2 + \frac{\beta_3}{2} \left\| z^{k+1} \odot o \odot |y| + \frac{\eta^k}{\beta_3} \right\|_2^2 \quad (25)$$

which can be simplified as

$$y^{k+1} = \arg \min_y \frac{1}{2} \left\| y - \frac{\beta_2 (u^{k+1} - f + \frac{\delta^k}{\beta_2})}{\beta_2 + \beta_3 (z^{k+1} \odot o)^2} \right\|_2^2 + \frac{z^{k+1} \odot o \odot \eta^k}{\beta_2 + \beta_3 (z^{k+1} \odot o)^2} \odot |y| \quad (26)$$

Subproblem (26) can be calculated by

$$y^{k+1} = \text{shrink} \left(\frac{\beta_2 (u^{k+1} - f + \frac{\delta^k}{\beta_2})}{\beta_2 + \beta_3 (z^{k+1} \odot o)^2}, \frac{z^{k+1} \odot o \odot \eta^k}{\beta_2 + \beta_3 (z^{k+1} \odot o)^2} \right) \quad (27)$$

where $\text{shrink}(x, y) = \text{sgn}(x) \cdot \max\{\|x\|_1 - y, 0\}$, and $\text{sgn}(\cdot)$ denotes the signum function.

Updating Lagrangian multipliers

Finally, the Lagrange multipliers are updated by the following

$$\begin{cases} \mu^{k+1} = \mu^k + \beta_1 (\nabla^\alpha u^{k+1} - x^{k+1}) \\ \delta^{k+1} = \delta^k + \beta_2 (u^{k+1} - f - y^{k+1}) \\ \eta^{k+1} = \eta^k + \beta_3 (z^{k+1} \odot o \odot |y^{k+1}|) \end{cases} \quad (28)$$

The proposed method is presented as Algorithm 2. And for this algorithm, we have two remarks.

Algorithm 2 solving the minimization problem (12).

- 1: input $f, \lambda_1 > 0, \lambda_2 > 0, \alpha, \text{Group size } K, \beta_1, \beta_2, \beta_3$
 - 2: initialization $u^0, x^0, v^0, z^0, y^0; \mu^0, \delta^0, \eta^0$
 - 3: iteration:
 - Compute u^{k+1} according to Eq. (19),
 - Compute x^{k+1} according to Eq. (21),
 - Compute v^{k+1} according to Eq. (21),
 - Compute z^{k+1} according to Eq. (24),
 - Compute y^{k+1} according to Eq. (27),
 - Update $\mu^{k+1}, \delta^{k+1}, \eta^{k+1}$ according to Eq. (28),
 - $k = k + 1$;
 - until a stopping criterion is satisfied.
-

Remark 1 When $\alpha = 1$, the fractional-order TV is reduced to the standard TV, so the Eq. (13) is degraded into the OGS-MCTV penalty in (Ji and Zhao, 2023). In the experimental section, we discuss in detail the effect of the value of α on the denoising performance of the proposed model.

Remark 2 When $K = 1$, the Eq. (13) is degraded into the MC penalty of the fractional-order TV term in (Chen and Zhao, 2023). Different K values lead to different denoising results, specific experiments are shown in the following section.

NUMERICAL EXPERIMENTS

In this section, we present several experimental results to verify the effectiveness of the proposed method for image denoising. The test image is real MR images, as shown in Fig. 1. All the test images are from the Department of Radiology, Maanshan People's Hospital, Maanshan, China. The experiment is under Windows 10 and MATLAB R2021a operating system, and the CPU is AMD R7 5800H 3.20GHz and 16GB RAM. MR images used for analysis were corrupted by salt-and-pepper noise levels of 30%, 50%, 70%. All denoising methods measure the quality of recovered images by Peak Signal-to-Noise Ratio (PSNR) and Structural Similarity (SSIM) indices, which reflect human subjective sensory and visual perception quality respectively (Irum *et al.*, 2015; Kuang *et al.*, 2018).

The stopping criterion for all tested algorithms is set to

$$\frac{\|u_{k+1} - u_k\|}{\|u_k\|} \leq 1 \times 10^{-4} \quad (29)$$

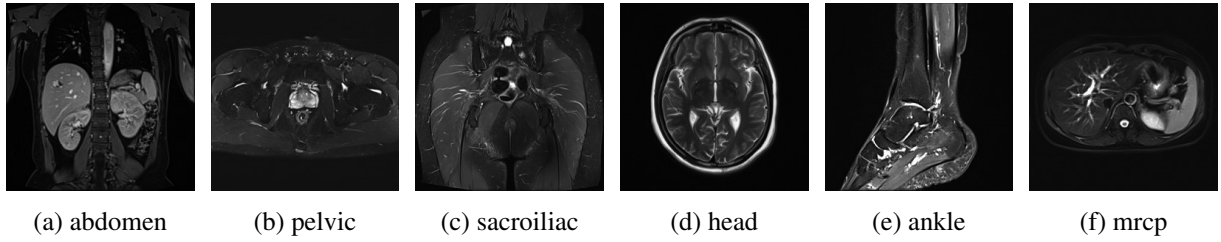


Fig. 1: MR images used for the experiments.

Table 1: The PSNR and SSIM values for denoised images by different methods when 30% noise level.

Noise level	Image	Denoised			
		HNHOTV-OGS	ℓ_1 -OGSTV	ℓ_0 -OGSTV	Proposed
30	abdomen	35.01/0.950	32.93/0.919	39.62/0.982	40.92/0.985
	pelvic	29.97/0.936	31.08/0.930	37.90/0.985	39.20/0.986
	sacroiliac	31.10/0.894	31.45/0.891	38.04/ 0.974	38.40/0.973
	head	29.19/0.955	29.53/0.943	36.51/0.989	37.62/0.991
	ankle	25.33/0.907	26.93/0.913	33.13/0.981	34.42/0.983
	mrcp	32.74/0.969	32.90/0.952	39.40/0.991	41.78/0.993

Table 2: The PSNR and SSIM values for denoised images by different methods when 50% noise level.

Noise level	Image	Denoised			
		HNHOTV-OGS	ℓ_1 -OGSTV	ℓ_0 -OGSTV	Proposed
50	abdomen	29.13/0.839	29.20/0.827	35.73/0.956	36.86/0.963
	pelvic	27.69/0.871	27.81/0.874	34.20/0.966	35.35/0.968
	sacroiliac	27.56/0.788	28.60/0.808	34.70/ 0.943	34.87/0.941
	head	24.07/0.873	24.84/0.873	32.59/0.973	33.72/0.977
	ankle	22.83/0.812	23.67/0.8287	29.67/0.956	30.93/0.960
	mrcp	28.01/0.910	28.74/0.901	35.77/0.977	38.06/0.981

Table 3: The PSNR and SSIM values for denoised images by different methods when 70% noise level.

Noise level	Image	Denoised			
		HNHOTV-OGS	ℓ_1 -OGSTV	ℓ_0 -OGSTV	Proposed
70	abdomen	21.51/0.499	26.00/0.679	31.85/0.900	32.46/0.909
	pelvic	24.42/0.745	25.66/0.807	30.45/0.930	31.53/0.932
	sacroiliac	23.27/0.597	25.93/0.715	31.19/0.886	30.90/0.878
	head	17.92/0.583	20.42/0.720	28.45/0.935	29.79/0.945
	ankle	19.26/0.603	21.38/0.697	26.28/0.907	27.24/0.914
	mrcp	23.04/0.714	25.53/0.811	31.98/0.949	33.93/0.957

Table 4: Denoising results of different MM iterations (N).

noise level	Image	N	PSNR	SSIM	Iter	Time(s)
30%	abdomen	1	40.81	0.984	638	4.980
		5	40.92	0.985	637	7.586
		10	16.79	0.980	1000	17.630
		100	14.95	0.977	1000	118.748
50%	head	1	33.71	0.976	1000	7.547
		5	33.72	0.977	1000	11.793
		10	29.06	0.975	1000	17.625
		100	33.51	0.976	1000	116.814

where u_{k+1} and u_k are the restored image at the current iterate and previous iterate respectively.

RESULTS AND ANALYSIS

The experimental results of our proposed model are compared with three related methods: ℓ_0 -OGSTV (Yin *et al.*, 2022), ℓ_1 -OGSTV (Liu *et al.*, 2015) and HNHOTV-OGS (Adam *et al.*, 2021). Their regularizers are closely related to the proposed method in this paper.

In the whole experiment, we fixed $\alpha = 1.9$, $K = 3$, $N = 5$, $\lambda_1 = 20$, $\lambda_2 = 30$, $b=200$, and other parameters were manually selected to obtain the most satisfactory restoration quality. For better comparison, HNHOTV-OGS and ℓ_0 -OGSTV keep within the scope of the authors suggest the parameters. For ℓ_1 -OGSTV, we manually select the parameters to get the best PSNR or SSIM value.

The effectiveness of this method on salt-and-pepper noise denoising is verified by experiments. Three different noise levels 30%, 50% and 70% are added to the test image respectively to generate each observed image. The obtained PSNR and SSIM values are shown in Table 1, Table 2 and Table 3.

In each table, we observed that even at different noise levels, compared with the denoising results of the other three methods, the PSNR and SSIM values of the proposed method were almost higher than those of the other three methods. Only about the picture “sacroiliac” performs slightly worse than ℓ_0 -OGSTV.

In Figs. 2-4, we show the comparison of the denoised images of the three methods for the MR Images “abdomen” and “pelvic” at 30% noise level,

“sacroiliac” and “head” at 50% noise level, and “ankle” and “mrpc” at 70% noise level, respectively. From the results, ℓ_1 -OGSTV image denoising effect is not ideal, there are still slight blocky artifacts, and some important texture edges are blurred. The closest competitor to our method is ℓ_0 -OGSTV, whose recovered images remove impulse noise well and reduce staircase artifacts due to the use of ℓ_0 -norm. However, as the noise level increased, our method still achieved better results. Because our method similarly uses the ℓ_0 -norm and combines the advantages of the overlapping group sparse fractional-order total variation and MC penalty term, it can well remove staircase artifacts and preserve detail edges even at high noise levels.

PARAMETER SENSITIVITY ANALYSIS

The parameters that affect the performance mainly include the fractional order α , the group size K , the number of MM iterations N , MC penalty parameter b and parameters λ_1 , λ_2 , and these parameters need to be carefully tuned to get more accurate results. Therefore, we selected some images to test under different noise conditions to demonstrate the sensitivity of the proposed model to these parameters.

Firstly, in order to test the sensitivity of iteration number N , other parameters are fixed. Table 4 shows the influence of different MM iteration number N on PSNR, SSIM, overall algorithm iteration number and time, and the best result is obtained when $N=5$.

The variation of the value of the group size K is important for the quality of the recovered image, and it can be obtained from Fig. 5 that when the group size $K=3$, the performance is the best, and the image quality

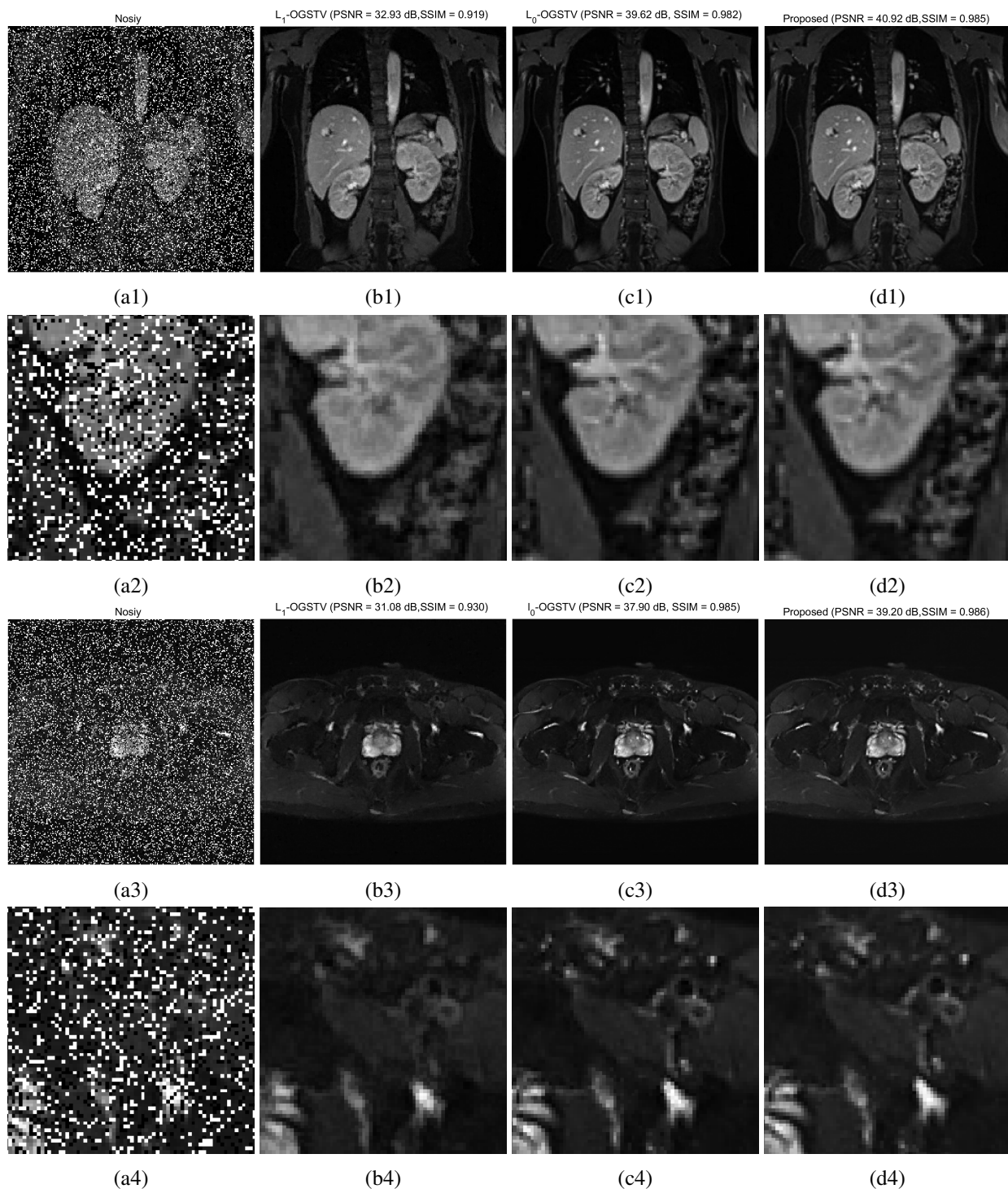


Fig. 2: The first and third lines are the recovered results for “abdomen” and “pelvic” with the 30% noise level, respectively, while the second and fourth lines show the fragments corresponding to the zoomed images. (a1)-(a4) noisy image, (b1)-(b4) ℓ_1 -OGSTV restored, (c1)-(c4) ℓ_0 -OGSTV restored, (d1)-(d4) proposed restored.

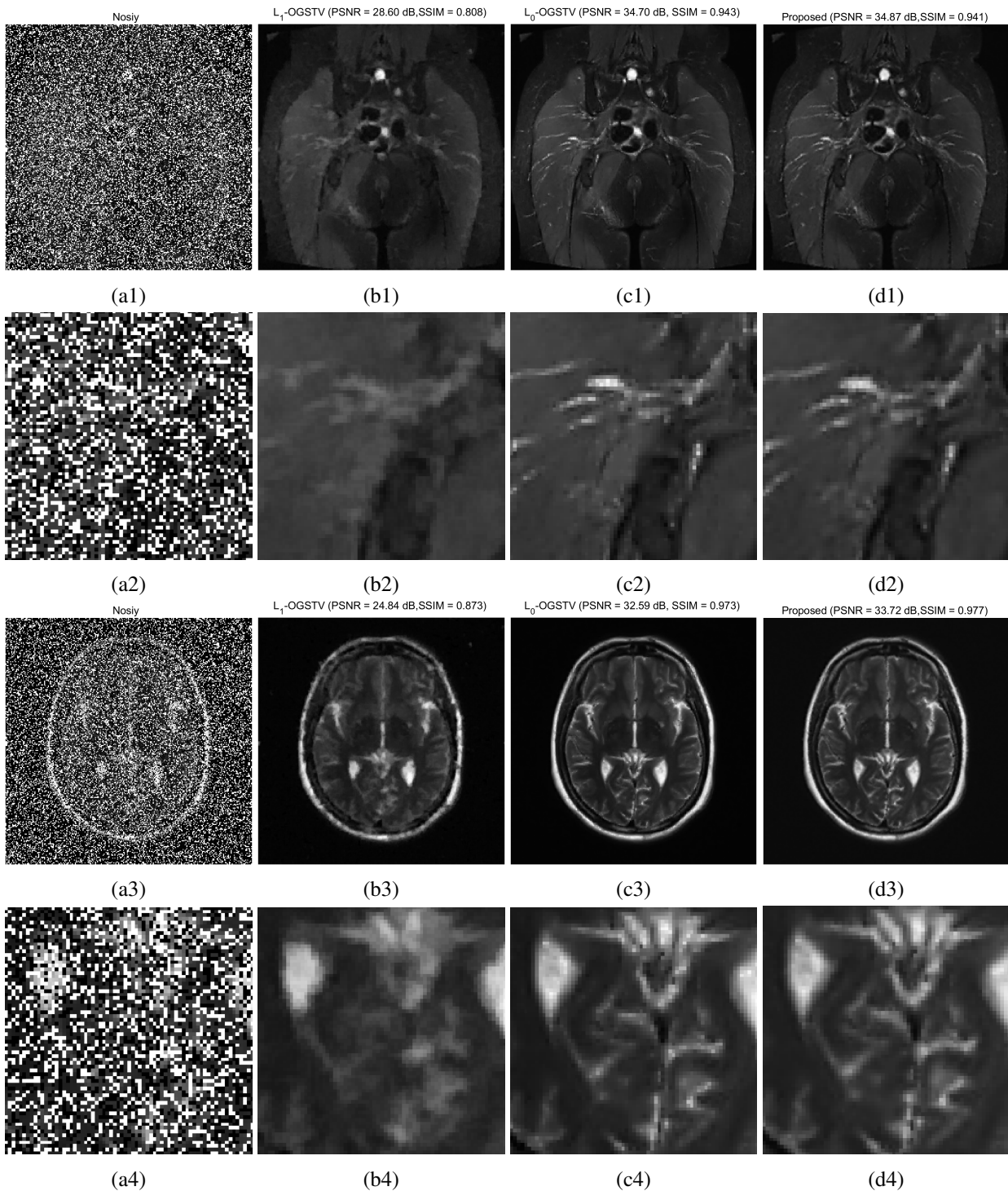


Fig. 3: The first and third lines are the recovered results for “sacroiliac” and “head” with the 50% noise level, respectively, while the second and fourth lines show the fragments corresponding to the zoomed images. (a1)-(a4) noisy image, (b1)-(b4) ℓ_1 -OGSTV restored, (c1)-(c4) ℓ_0 -OGSTV restored, (d1)-(d4) proposed restored.

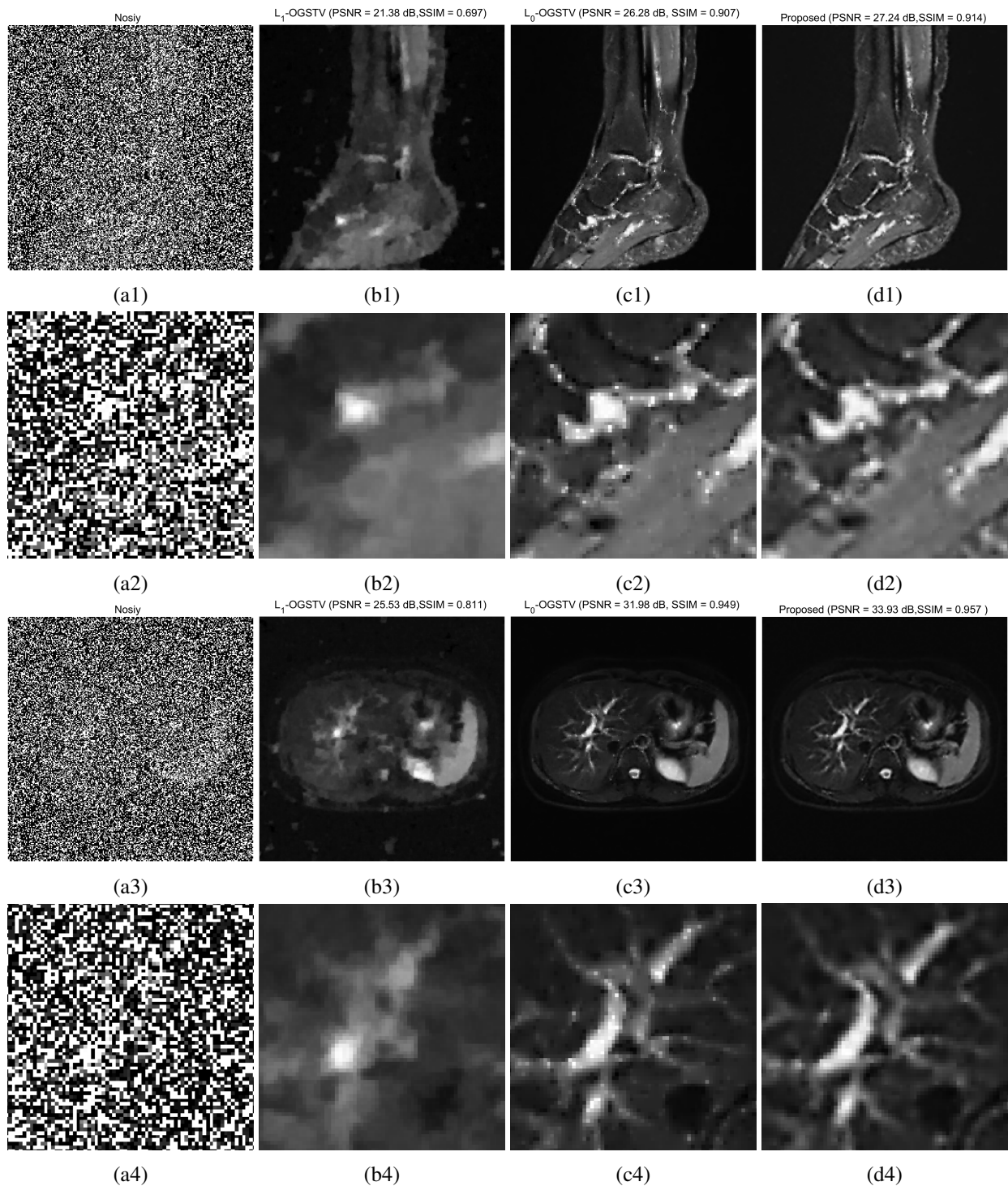


Fig. 4: The first and third lines are the recovered results for “ankle” and “mrcp” with the 70% noise level respectively, while the second and fourth lines show the fragments corresponding to the zoomed images. (a1)-(a4) noisy image, (b1)-(b4) ℓ_1 -OGSTV restored, (c1)-(c4) ℓ_0 -OGSTV restored, (d1)-(d4) proposed restored.

does not continue to improve if the K value continues to increase.

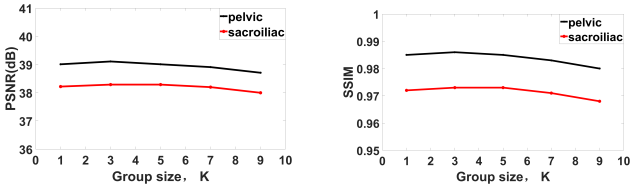


Fig. 5: PSNR and SSIM values for images denoised by my method with different K (set 30% salt-and-pepper noise, inner iteration $N = 5$).

In our experiment, the range of values about fractional order α is $1 \leq \alpha < 2$. In Fig. 6, we test two images at 30% and 50% noise levels respectively. The figures show the PSNR and SSIM values increase with the α value. Therefore, $\alpha = 1.9$ can obtain the best PSNR and SSIM results.

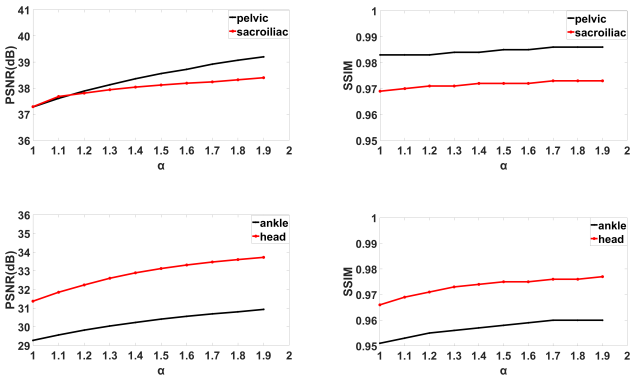


Fig. 6: PSNR and SSIM values for images denoised by my method with different α (set 30% and 50% salt-and-pepper noise, inner iteration $N = 5$, group size $K=3$).

In this paper, the parameters λ_1 and λ_2 respectively control the weight of the overlapping group sparse fractional-order total variation and MC penalty terms. Because the new regularizer is based on the overlapping group sparse fractional-order total variational minus the MC penalty term, the new regularizer is more successful in generating sparsity. According to the experimental test, when λ_1 and λ_2 are [20, 30], the denoising effect of the model is relatively ideal. In Fig. 7, the recovery results of “abdomen” at 50% noise level and “head” at 70% noise level are shown for different values of λ_1 and λ_2 , respectively, where (c1)-(c2) perform the best, and we set $\lambda_1=20$ and $\lambda_2=30$.

Finally, the analysis is about the parameter b in the MC penalty term. As shown in Fig. 8, we test the effect of different b values on PSNR and SSIM values at two noise levels, and it is observed that $b=200$ is the optimal choice.

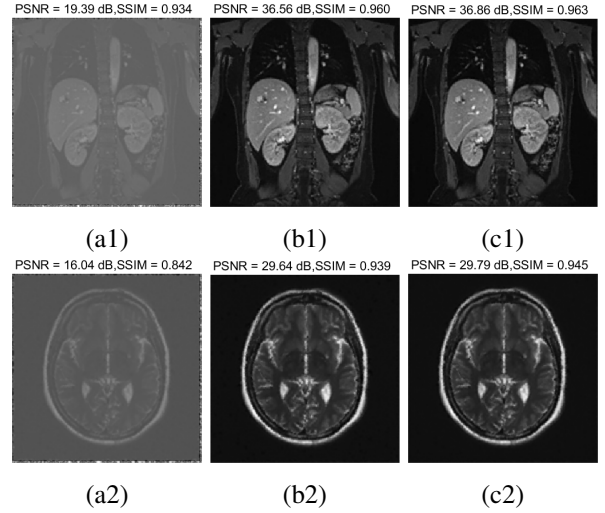
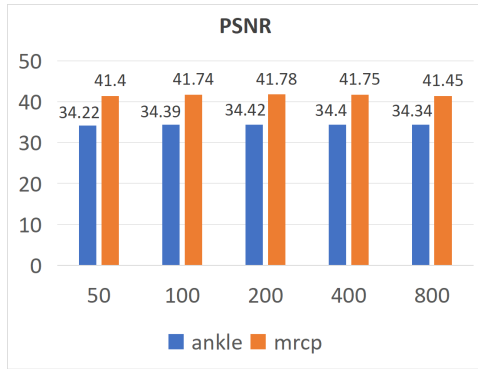


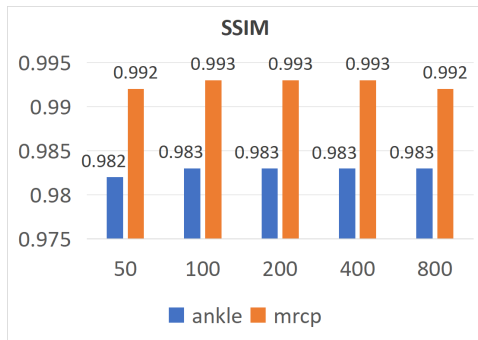
Fig. 7: Denoising results of different λ_1, λ_2 for “abdomen” (50% noise level) and “head” (70% noise level). (a1)-(a2) $\lambda_1 > \lambda_2$, (b1)-(b2) $\lambda_1 = \lambda_2$, (c1)-(c2) $\lambda_1 < \lambda_2$.

CONCLUSION

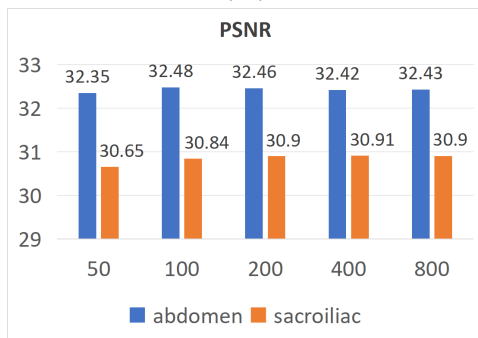
In this paper, we propose a novel denoising model for MR images aimed at effectively removing impulse noise and staircase artifacts. We demonstrate the effectiveness of using the ℓ_0 -norm as a data fidelity term to eliminate impulse noise, while the combination of the overlapping group sparse fractional-order total variation and MC penalty as regularizers can mitigate staircase artifacts and preserve important edges. To solve the proposed model, we employ the alternating direction method of multipliers. Numerical experiments validate that our proposed method outperforms three alternative methods in terms of PSNR and SSIM across varying levels of noise. In future work, we aim to extend our proposed method to address other types of noise and reduce computational time.



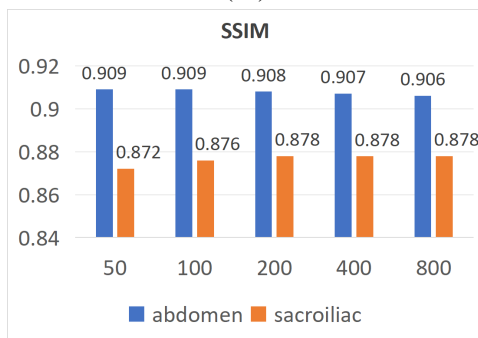
(a1)



(b1)



(a2)



(b2)

Fig. 8: Denoising results of different b . (a1)-(b1) 30% noise level, (a2)-(b2) 70% noise level.

ACKNOWLEDGMENTS

This work was supported in part by the Natural Science Foundation of the Anhui Higher Education Institutions of China (Grant Nos. 2023AH040149), the Anhui Provincial Natural Science Foundation (Grant No. 2208085MF168), the Key Research and Development Plan of Anhui Province (Grant No. 2022e07020065), and the Ma'anshan City Science and Technology Planning Project (Grant No. YL-2022-5).

REFERENCES

- Adam T, Paramesran R, Mingming Y, Ratnavelu K (2021). Combined higher order non-convex total variation with overlapping group sparsity for impulse noise removal. *Multimed Tools Appl* 80:18503–30.
- Bhutto J A, Khan A, Rahman Z (2023). Image restoration with fractional-order total variation regularization and group sparsity. *Mathematics* 11:3302.
- Boyd S, Parikh N, Chu E, Peleato B, Eckstein J (2011). Distributed optimization and statistical learning via the alternating direction method of multipliers. *Found Trends® Mach Learn* 3:1–122.
- Chan R H, Dong Y, Hintermüller M (2010). An Efficient Two-Phase L^1 -TV Method for Restoring Blurred Images with Impulse Noise. *IEEE Trans Image Process* 19:1731–39.
- Chen X, Zhao P (2023). Image denoising based on the fractional-order total variation and the minimax-concave. *Signal Image Video Process*, 1–8.
- Du H, Liu Y (2018). Minmax-concave total variation denoising. *Signal Image Video Process* 12:1027–34.
- Gao Y, Liu F, Yang X (2018). Total generalized variation restoration with non-quadratic fidelity. *Multidimens. Syst Signal Process* 29:1459–84.
- Ge Y, Xue W, Xu Y, Huang J, Gu X (2023). Magnetic Resonance Image Denoising Based on Laplacian Prior Sparsity Constraint and Nonconvex Second-Order TV Penalty. *Image Anal Stereol* 42:119–32.
- Hestenes M R (1969). Multiplier and gradient methods. *J Optim Theory Appl* 4(5):303–20.

- Irum I, Shahid M A, Sharif M, Raza M (2015). A Review of Image Denoising Methods. *J Eng Sci Technol Rev* 8:41–8.
- Ji M, Zhao P (2023). Image restoration based on the minimax-concave and the overlapping group sparsity. *Signal Image Video Process* 17:1733–41.
- Kuang S, Chao H, Li Q (2018). Matrix completion with capped nuclear norm via majorized proximal minimization. *Neurocomputing* 316:190–201.
- Lian W, Liu X (2023). Non-convex fractional-order TV model for impulse noise removal. *J Comput Appl Math* 417:114615.
- Liu G, Huang T Z, Liu J, Lv X G (2015). Total variation with overlapping group sparsity for image deblurring under impulse noise. *PloS One* 10:e0122562.
- Liu J, Huang T Z, Selesnick I W, Lv X G, Chen P Y (2014). Image restoration using total variation with overlapping group sparsity. *Inf Sci* 24:2057–75.
- Rahman Chowdhury M, Zhang J, Qin J, Lou Y (2020). Poisson image denoising based on fractional-order total variation. *Inverse Probl Imaging Syst* 14:77–96.
- Rudin L I, Osher S, Fatemi E (1992). Nonlinear total variation based noise removal algorithms. *Physica D* 60:259–68.
- Selesnick I (2017). Total variation denoising via the Moreau envelope. *IEEE Signal Process Lett* 24:216–20.
- Selesnick I W, Chen P Y (2013). Total variation denoising with overlapping group sparsity. In *Proc IEEE Int Conf Acoust Speech Signal Process*, 5696–700.
- Shen M, Li J, Zhang T, Zou J (2021). Magnetic resonance imaging reconstruction via non-convex total variation regularization. *Int J Imaging Syst Technol* 31:412–24.
- Shi M, Han T, Liu S (2016). Total variation image restoration using hyper-Laplacian prior with overlapping group sparsity. *Signal Process* 126:65–76.
- Sun T, Liu X (2023). Non-convex TGV regularized ℓ_0 -norm fidelity model for impulse noise removal. *Signal Process*, 109125.
- Wang Y, Yin W, Zeng J (2019). Global convergence of ADMM in nonconvex nonsmooth optimization. *Journal of Scientific Computing. J Sci Comput* 78:29–63.
- Wu C, Tai X C (2010). Augmented Lagrangian method, dual methods, and split Bregman iteration for ROF, vectorial TV, and high order models. *SIAM J Imaging Sci* 3: 300–39.
- Yang J, Zhang Y, Yin W (2009). An efficient TVL1 algorithm for deblurring multichannel images corrupted by impulsive noise. *SIAM J Sci Comput* 31:2842–65.
- Yin M, Adam T, Paramesran R, Hassan M F (2022). An ℓ_0 -overlapping group sparse total variation for impulse noise image restoration. *Signal Process Image Commun* 102:116620.
- Yuan G, Ghanem B (2017). ℓ_0 TV: A Sparse Optimization Method for Impulse Noise Image Restoration. *IEEE Trans Pattern Anal Mach Intell* 41:352–64.
- Zhang J, Wei Z, Xiao L (2012). Adaptive fractional-order multi-scale method for image denoisings. *J Math Imaging Vision* 43:39–49.
- Zhou M, Zhao P (2021). Enhanced total generalized variation method based on moreau envelope. *Multimed Tools Appl* 80:19539–66.
- Zhu J, Wei J, Hao B (2022). Fast algorithm for box-constrained fractional-order total variation image restoration with impulse noise. *IET Image Process* 16:3359–73.